Feshbach-resonance-mediated positron annihilation in small molecules

J. A. Young* and C. M. Surko
Department of Physics, University of California, San Diego, 9500 Gilman Drive, La Jolla, California 92093-0319, USA
(Received 21 June 2008; published 3 September 2008)

Large positron annihilation cross sections have been observed for a variety of molecules at various energies below the threshold for positronium formation. These large values are due to vibrational Feshbach resonances (VFRs), in which the positron attaches to the molecule while exciting a vibration. This leads to rates of annihilation far greater than those expected for a simple collision. The dependence of the annihilation rate on incident positron energy can be used to deduce positron-molecule binding energies. Presented here is a comprehensive study of resonant annihilation in small molecules (e.g., hydrocarbons with one or two carbon atoms). In some cases, only fundamental vibrations are important, and theory correctly predicts the annihilation rates as a function of incident positron energy. In other cases, combination and overtone vibrations are shown to support Feshbach resonances. In the subset of these cases where the positron-molecule coupling strengths can be determined for these combination modes, theoretical predictions are in agreement with the measurements. Finally, there are species that do not exhibit VFRs, such as carbon dioxide. This is interpreted as evidence that positrons bind very weakly or not at all to these targets. Several of these molecules exhibit a variety of behaviors that are presently unexplained. The implications of the results presented here for more comprehensive theories of positron annihilation on molecules are discussed.

DOI: 10.1103/PhysRevA.78.032702 PACS number(s): 34.80.Uv, 34.50.−s, 78.70.Bj, 71.60.+z

I. INTRODUCTION

In spite of their importance in many areas of science and technology, including medicine, materials science, and fundamental physics, positron interactions with simple targets such as atoms and molecules are not well understood [1–3]. We consider here the process of annihilation below the positronium formation threshold, which has puzzled and intrigued researchers for more than four decades, beginning with the seminal work of Paul and Saint Pierre [4–7].

It is now known that positrons with energies below the threshold for positronium formation can attach to many, if not most, hydrocarbon molecules [3,8–13]. As a result, they exhibit greatly enhanced rates of annihilation, beyond those expected on the basis of simple collisions. This occurs via vibrational Feshbach resonances (VFRs), in which an incident positron excites a molecular vibration and becomes attached to the molecule. This process increases the overlap of the positron and electron densities, thereby increasing greatly the probability of annihilation. The ultimate fate of the positron in such a resonance is determined by a competition between annihilation and reemission from the target as a result of deexcitation of a molecular vibrational mode.

Annihilation rates λ for atoms and molecules in the gas phase are typically expressed in terms of a normalized rate Z_{eff}, which is the ratio of λ for a given density of molecules, n_m, to the rate for the same density of free electrons [2]. Specifically, $Z_{\text{eff}}=\lambda/(\pi r_0^2 c n_m)$, where c is the speed of light and r_0 is the classical electron radius. For a simple scattering event, it is expected that $Z_{\text{eff}} \lesssim Z$, the total number of electrons in the atom or molecule [4–6,14], and Z_{eff} can be thought of as the number of electrons participating in the annihilation process. However, for many molecules $Z_{\text{eff}} \gg Z$ because of VFR-mediated positron attachment [14–16].

Positron attachment via the vibrational Feshbach resonance mechanism can be most easily understood by studying annihilation in molecules with only a few degrees of freedom, all of which are dipole coupled to the incident positron [16]. A successful theory has now been developed for this case, which is in quantitative agreement with the experimental measurements for annihilation in methyl halide molecules (i.e., CH_3X, where X is a halogen atom) [16,17]. Presented here are data for a variety of other small molecules (e.g., hydrocarbons with one or two carbon atoms) in which the annihilation can be understood, at least qualitatively, within a similar theoretical framework. The discussion is restricted primarily to cases in which there are no additional enhancements due to intramolecular vibrational energy redistribution (IVR), which can enhance annihilation rates by additional orders of magnitude [11–13]. Also discussed here are cases in which combinations and overtones of the normal modes of the molecule contribute significantly to the observed annihilation. Finally, data are presented for molecules that do not exhibit identifiable VFRs. Several of these molecules, such as H_2O, CO_2, and CH_4, do however exhibit a variety of other effects. The results presented here provide insight into the conditions required for positron-molecule attachment and VFR-induced annihilation.

This paper is organized in the following way. An overview is presented of the theory of VFR-mediated annihilation in small molecules [16]. The experimental procedures used in these studies are briefly described. Data are then presented, and their implications for more complete theories of the annihilation process and other open questions are discussed.

*Present address: Jet Propulsion Laboratory, 4800 Oak Grove Drive, Pasadena, California 91109.

II. THEORY OF POSITRON ANNIHILATION IN SMALL MOLECULES

Gribakin and Lee have developed a quantitative theory of Z_{eff} spectra due to infrared-active modes in small molecules [16]. It provides a framework for understanding much of the annihilation behavior observed in these species. Resonant annihilation is assumed to occur via positron capture followed by annihilation. Each vibrational mode ν contributes a Breit-Wigner resonance, namely,

$$Z_{\mathrm{eff}}^{(\mathrm{res})}(\epsilon)=\frac{1}{kr_0^2c}\sum_{\nu}\frac{b_\nu\Gamma_\nu^a\Gamma_\nu^e}{(\epsilon-\omega_\nu+\epsilon_b)^2+\Gamma_\nu^2/4}, \tag{1}$$

where Γ_ν^a is the *internal* annihilation rate, Γ_ν^e is the elastic capture rate, Γ_ν is the total rate for all processes including escape via the elastic scattering channel, ϵ_b is the binding energy, ω_ν is the vibrational mode energy, b_ν is the mode degeneracy, ϵ is the incident positron energy, and k is the positron momentum. Atomic units are used for this and the other theoretical expressions in this paper. A number of approximations are then applied to determine these parameters. The wave function of the bound positron is assumed to be s wave in character, such as that which would arise from a single zero-range potential [18],

$$\varphi_0(r)=A\frac{e^{-\kappa r}}{r}. \tag{2}$$

This corresponds to a positron scattering length $1/\kappa$ and a binding energy $\epsilon_b=\kappa^2/2$, with a normalization factor $A=\sqrt{\kappa/2\pi}$. Calculation of the positron capture width is done using the Born-dipole approximation for the positron-molecule coupling. The initial state is assumed to be a plane wave $e^{i\mathbf{k}\cdot\mathbf{r}}$ for the positron and a ground state wave function Φ_0 for the molecular electrons and nuclei. The final state is a bound positron with wave function $\varphi_0(r)$ and a vibrationally excited molecule in state Φ_ν. Initial and final states are coupled via a potential based on the dipole operator $\hat{\mathbf{d}}$. The resulting transition amplitude $A_{\nu\mathbf{k}}$ is

$$A_{\nu\mathbf{k}}=\langle\varphi_0(r)\Phi_\nu|\frac{\hat{\mathbf{d}}\cdot r}{r^3}|e^{i\mathbf{k}\cdot\mathbf{r}}\Phi_0\rangle=\langle\varphi_0(r)|\frac{\mathbf{d}_\nu\cdot\mathbf{r}}{r^3}|e^{i\mathbf{k}\cdot\mathbf{r}}\rangle, \tag{3}$$

where

$$\mathbf{d}_\nu=\langle\Phi_\nu|\hat{\mathbf{d}}|\Phi_0\rangle. \tag{4}$$

The transition dipole moment $\mathbf{d}_\nu$ for the coupling to a vibrational mode ν can be obtained from either infrared absorption data or computed using standard software (e.g., GAMESS [19]). In particular, the infrared absorption cross section is proportional to $\omega_\nu d_\nu^2$. The elastic capture rate Γ_ν^e is then given by

$$\Gamma_\nu^e=2\pi\int|A_{\nu\mathbf{k}}|^2\delta(k^2/2-\omega_\nu+\epsilon_b)\frac{d^3k}{(2\pi)^3}=\frac{16\omega_\nu d_\nu^2}{27}h(\xi) \tag{5}$$

where

$$h(\xi)=\xi^{3/2}(1-\xi)^{-1/2}\left[{}_2F_1\left(\frac{1}{2},1;\frac{5}{2};-\xi/(1-\xi)\right)\right]^2 \tag{6}$$

and $\xi=1-\epsilon_b/\omega_\nu$.

The final expression for $A_{\nu\mathbf{k}}$ is calculated analytically and involves the hypergeometric function ${}_2F_1$ [16]. The function $h(\xi)$ has a single maximum of 0.75 at $\xi=0.89$ and gradually drops to zero at $\xi=0$ and 1. Thus, Γ_ν^e is essentially proportional to the infrared absorption cross section for the ν^{th} mode.

The remaining rate, Γ_ν^a, is that for the dominant 2-γ annihilation and is determined by the positron-electron overlap density ρ_{ep}, defined by

$$\Gamma_\nu^a=\pi r_0^2c\rho_{ep}. \tag{7}$$

Assuming a diffuse positron wave function with strong core repulsion, the electron and positron wave functions can be expected to overlap predominantly near the surface of the molecule [14,15]. This assumption is consistent with γ-ray spectroscopy results showing that positrons preferentially annihilate on the valence electrons [20]. Therefore, given an electron density $\rho_e(R)$ and a long-range positron wave function like that described in Eq. (2), the positron-electron overlap is simply

$$\rho_{ep}=\frac{F}{2\pi}\kappa, \tag{8}$$

where F is a constant. Values of Γ^a and κ have been calculated for several atoms using the stochastic variational method, assuming fixed cores [21]. These values are found to be linearly related to each other, giving an empirical value of $F\approx0.66$ [15,22].

Neglecting other channels, the total rate $\Gamma_\nu=\Gamma_\nu^e+\Gamma_\nu^a$ is much smaller than the experimental width of the positron beam [which is about 40 meV full width at half maximum (FWHM)]. Hence, when the distribution function of the positron beam, $f(\epsilon)$, is taken into account, the expression for the resonant part of Z_{eff} can be written as

$$Z_{\mathrm{eff}}^{(\mathrm{res})}(\epsilon)=2\pi^2\sum_\nu\frac{\rho_{ep}}{k_\nu}\frac{b_\nu\Gamma_\nu^e}{\Gamma_\nu}f(\epsilon-\epsilon_\nu)\approx\pi F\sum_\nu g_\nu\frac{b_\nu\Gamma_\nu^e}{\Gamma_\nu}f(\epsilon-\epsilon_\nu), \tag{9}$$

where

$$g_\nu=\kappa/k_\nu=\sqrt{\epsilon_b/\epsilon_\nu} \tag{10}$$

and $\epsilon_\nu=\omega_\nu-\epsilon_b$.

Typically, $\Gamma_\nu^e\gg\Gamma_\nu^a$, so that the ratio $\Gamma_\nu^e/\Gamma_\nu\simeq1$, in which case the final expression is essentially independent of the capture rate. Hence, the peak heights are determined *entirely* by the product of factors Fg_ν. This is a key result, which is remarkably useful in interpreting a broad class of experimental data.

There is also a relatively small contribution from direct annihilation, $Z_{\mathrm{eff}}^{(\mathrm{dir})}$ [14], namely, "pick-off" annihilation that occurs during ordinary elastic scattering. At low energies, $Z_{\mathrm{eff}}^{(\mathrm{dir})}$ can be expressed in terms of the overlap parameter F and the elastic cross section σ_{el} as

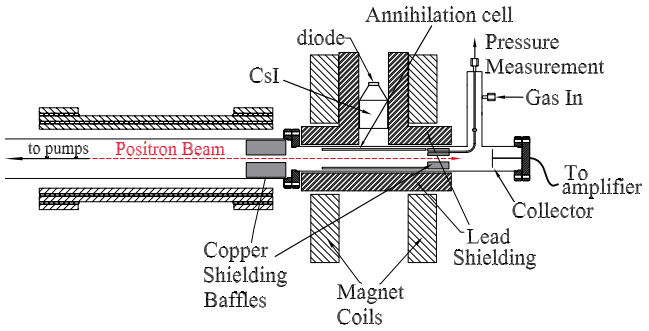

FIG. 1. (Color online) Schematic diagram of the experimental apparatus used for studies of test gases at 300 K. See text for details.

$$Z_{\mathrm{eff}}^{(\mathrm{dir})} = F\frac{\sigma_{\mathrm{el}}}{4\pi} + Z_{\mathrm{eff}}^{0} = \frac{F}{\kappa^2 + k^2} + Z_{\mathrm{eff}}^{0}, \tag{11}$$

where Z_{eff}^{0} is the small, constant contribution due to the overlap between the incident positron and molecular electron densities (i.e., typically, $Z_{\mathrm{eff}}^{0} \sim Z$) [10,14]. When Eq. (11) is convolved with the experimentally measured energy distribution of the positron beam, the maximum achievable Z_{eff} for thermal positrons at 300 K is ~1000 [14,15].

III. EXPERIMENTAL PROCEDURES

The experimental procedures used to measure molecular annihilation rates as a function of positron energy have been discussed in detail elsewhere [8–10]. The experimental apparatus is shown schematically in Fig. 1.

Moderated positrons are accumulated and cooled in a three-stage buffer-gas accumulator using a gas mixture of N_2 and CF_4. Pulses of positrons from the trap are magnetically guided through the cylindrical electrode of a cell filled with the test gas. The energy of the incident positrons is adjusted by varying the electrical potential of the gas cell. The total positron energy is obtained from retarding potential analyzer measurements of the parallel energy distribution (25 meV, FWHM), assuming a Maxwellian velocity distribution ($T \sim 25$ meV) in the plane perpendicular to the magnetic field [16]. Thus, 12 meV is added to the mean parallel energies so that the positions of the peak maxima correspond to values of the total positron energy. This amounts to a 4 meV reduction in the resonant peak shift as compared to the correction procedure used previously (e.g., in Refs. [9,10,23]). Further details of the beam energy distribution are described in Ref. [16].

Spectra for Z_{eff} are plotted as a function of total positron energy ϵ. The widths and shapes of the observed resonances are dominated completely by the energy distribution of the incident positron beam of width δ. One consequence is that the magnitudes of peaks in Z_{eff} measured in this way are smaller than those of the actual resonances by a factor of Γ_ν/δ.

The species studied here are gases with appreciable vapor pressures at 300 K. Test-gas pressure is controlled by a piezoelectric valve. The voltage on this piezovalve is regulated by a proportional-integral-derivative controller, using the pressure read by a capacitance manometer as an input. Typically, the pressure can be set with microtorr precision, limited only by the accuracy of the manometer and the response of the piezovalve. Single quanta from 2γ annihilation events are detected using a CsI detector. Positron pulses are allowed to pass through the gas cell four or five times while annihilation events are recorded, with the total scattering kept below 15%. Absolute values of Z_{eff} are obtained from measurements of the positron pulse strength, the path length and the test-gas pressure to within an absolute accuracy of approximately 20%.

IV. ANNIHILATION DUE TO MODE-BASED VFR: 1-HALOMETHANES AND ETHANOL

Halomethanes have a small number of vibrational modes which reduces the computational complexity. This also provides greater energy separation of the modes, in turn allowing better resolution of individual features. The resonant peaks in Z_{eff} are associated with the vibrational modes, all of which have strong electric dipole transitions.

Shown in Fig. 2 are energy-resolved Z_{eff} spectra for methyl fluoride (CH_3F), methyl chloride (CH_3Cl), and methyl bromide (CH_3Br) [10]. The vertical bars below each spectrum indicate the positions of the infrared- and Raman-active vibrational modes according to the NIST webbook [24]. All of these spectra exhibit VFRs in the form of two or more peaks which correlate strongly with the positions of infrared (ir) absorption resonances. The highest-energy peak in each spectrum is due to the C-H stretch vibrational modes. The stronger, low-energy peaks are due to the C-H bend modes and C-X modes (i.e., where X is the halogen). The lower-energy modes are spread further apart for the larger halogens, resulting in a broader spectrum of low-energy peaks. In CH_3Cl, one can distinguish three classes of modes: the C-H stretch, C-H bend, and the C-X modes, although it is not possible to distinguish the symmetric and asymmetric modes in each class. It is also not possible to distinguish the C-X stretch and bend modes.

As the size of the halogen increases, its Z_{eff} peaks increase in magnitude and shift to lower energies, indicating increasing positron-molecule binding energies. The corresponding binding energies are ~25 meV for CH_3Cl and ~40 meV and for CH_3Br. The binding energy for CH_3F is too small to be resolved. In fact, the C-H stretch peak is shifted *above* the position of the C-H stretch energy for the neutral molecule. Since negative binding is impossible for a VFR, it appears that the energy of the C-H stretch mode is shifted upward, which is perhaps due to the presence of the positron.

As can be seen by examining the data in Fig. 2(b), the CH_3Cl molecule has a positron binding energy of ~25 meV. According to Eqs. (7) and (8), $\Gamma^a = 0.15$ μeV. In contrast, the Γ_ν^e are of the order of 0.1 meV [16]. Table I shows $\Gamma_\nu^e/h(\xi)$ and $h(\xi)$ for each fundamental vibration of CH_3Cl, confirming that Γ_ν^e is consistently much larger than Γ^a.

As shown in Fig. 3, the theoretical predictions for the methyl halides from Eqs. (9) and (11) agree very well with the experimental data [10]. The only free parameter in this

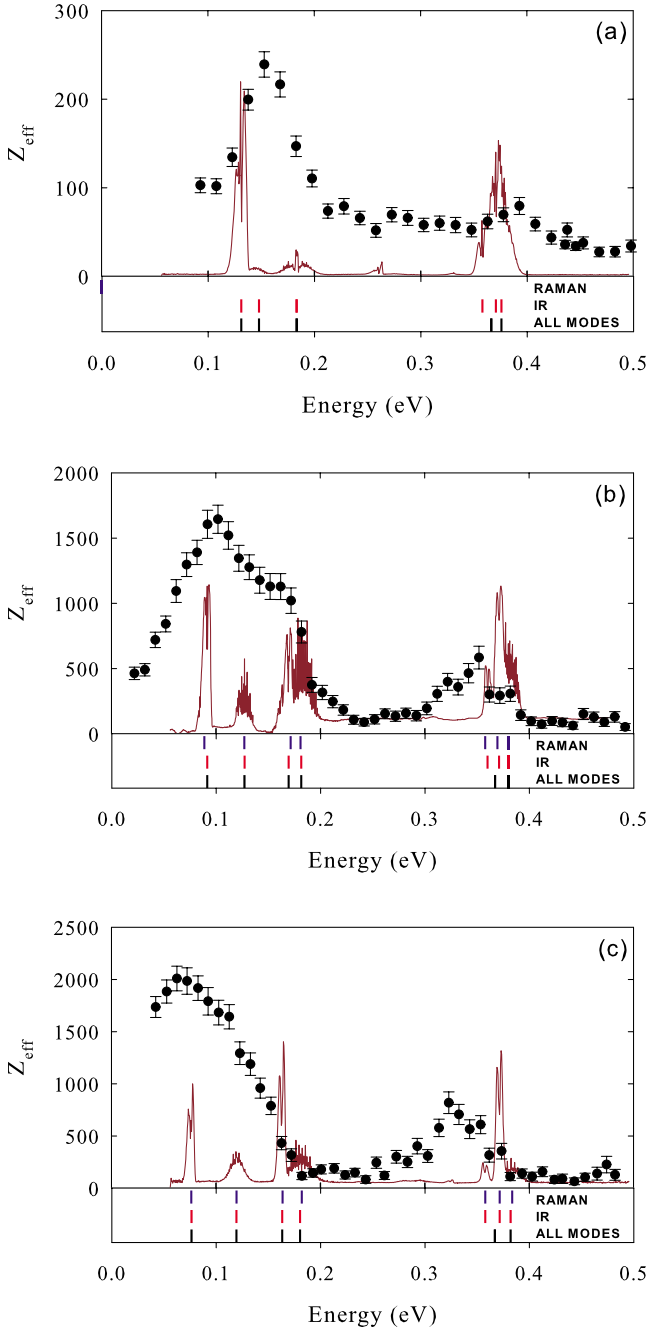

FIG. 2. (Color online) (●) Z_{eff} for (a) methyl fluoride, (b) methyl chloride, and (c) methyl bromide. The solid curves indicate the normalized infrared absorption spectra, and the vertical bars beneath each plot indicate the positions of the vibrational modes (from NIST [24]).

model is the binding energy, which can be determined from experiment, with the exception of CH_3F. In that case, a small binding energy of 0.3 meV was assumed which results in a best fit to the data.

Many of the observed trends are consistent with this theory. The fact that the low-energy peaks are larger than the high-energy peaks is due entirely to the factor $g_\nu = \sqrt{\epsilon_b/\epsilon_\nu}$, as is the increase of Z_{eff} with positron binding energy. The overall magnitude is determined by F and g_ν alone. This is due to the cancellation of Γ^e_ν with Γ_ν for the infrared-active fundamental vibrations. While this cancellation provides robust predictions, it also means that little information about resonant capture rates can be gleaned from the Z_{eff} spectra.

TABLE I. Physical parameters of CH_3Cl modes used in the calculation of Born-dipole elastic rates [16].

Mode	Symmetry	ω_ν (meV)	g_ν	d_ν (a.u.)	$h(\xi)$	$\Gamma^e_\nu/h(\xi)$ (μeV)
ν_1	a_1	363	1	0.0191	0.73	78.2
ν_2	a_1	168	1	0.0176	0.75	30.6
ν_3	a_1	91	1	0.0442	0.63	105
ν_4	e	373	2	0.0099	0.72	22.0
ν_5	e	180	2	0.0162	0.75	27.9
ν_6	e	126	2	0.0111	0.70	9.09

In order to provide a more stringent test of the Gribakin-Lee VFR model, experiments with *deuterated* methyl halides were also performed [17]. While deuteration lowers the frequency of many of the modes, the positron binding energies are expected to be unchanged. This has been confirmed by experiments on a number of hydrocarbons [8,9,12,25]. Using the binding energies determined from Fig. 2 for CH_3Cl and CH_3Br, the theoretical predictions for their deuterated analogs are fully constrained.

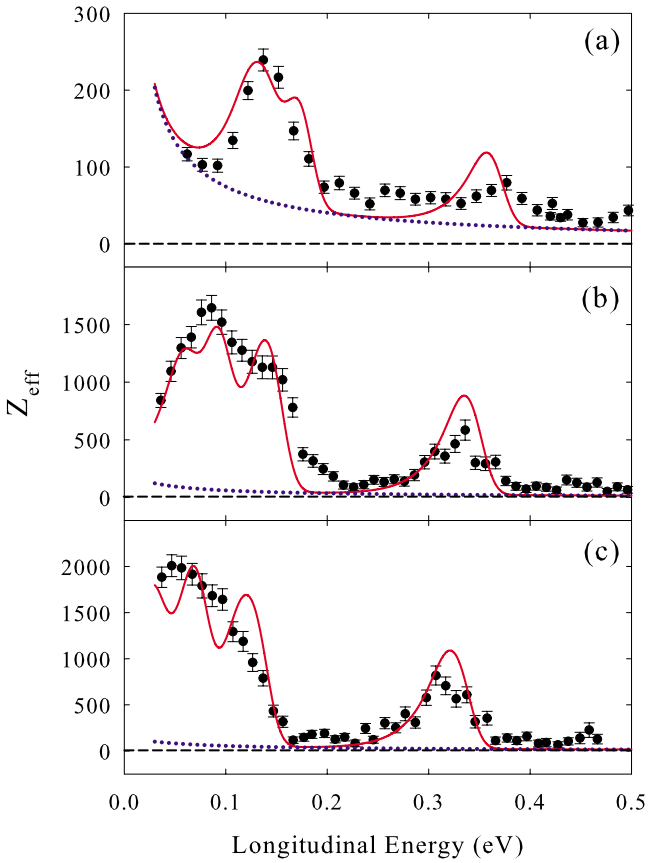

FIG. 3. (Color online) Z_{eff} data (●) compared with the Gribakin-Lee model for (a) methyl fluoride, (b) methyl chloride, and (c) methyl bromide, using positron-molecule binding energies of 0.3, 25, and 40 meV, respectively [16]. The solid curves are the predictions of the model, with the dotted curves indicating the nonresonant (direct) contributions to Z_{eff}.

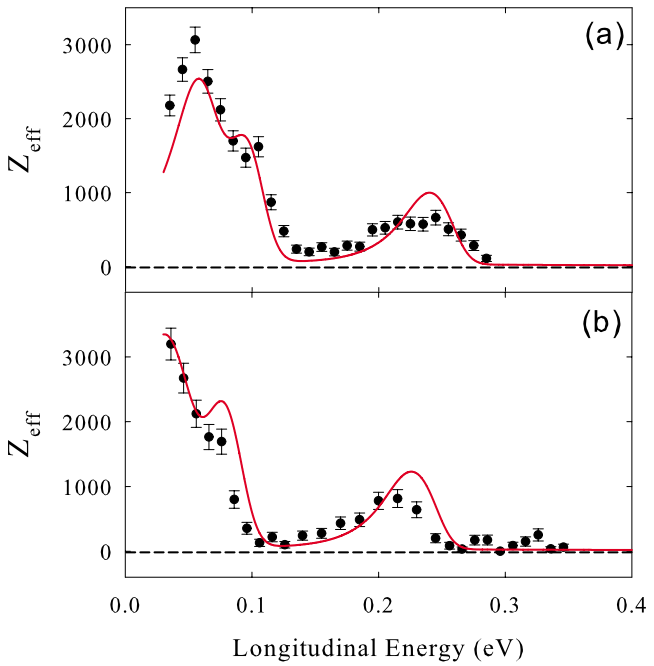

FIG. 4. (Color online) Energy-resolved Z_{eff} (●) for (a) deuterated methyl chloride and (b) deuterated methyl bromide. The predictions of Gribakin-Lee theory from Ref. [26], with *no* fitted parameters, are shown by the solid curves.

Figure 4 shows the Z_{eff} spectra of CD_3Cl and CD_3Br compared with the theoretical predictions. The agreement between experiment and theory is very good for CD_3Cl. In CD_3Br, the peak heights match well, indicating that the choice of binding energy is close to the right value. There is a slight mismatch in the peak positions in CD_3Br of about 12 meV, which is approximately the uncertainty in the positron-beam energy calibration.

Overall, the data in Fig. 4 provide excellent confirmation of the theory with *no* free parameters. The theory provides a robust understanding of the VFR mechanism in small molecules. It has now been extended in various ways to explain the Z_{eff} spectra for molecules of increasing size and complexity [12,13]. For example, we have shown recently that the scaling factor $g=\sqrt{\epsilon_b/\epsilon_\nu}$ generally determines the dependence of Z_{eff} on binding energy, even for large molecules [12,13].

As we discuss below, most hydrocarbon molecules with more than one carbon atom exhibit phenomena beyond mode-based VFRs. However, another molecule that is amenable to straightforward application of the simplest version of the theory is ethanol (C_2H_5OH). The energy-resolved Z_{eff} spectrum of this molecule is shown in Fig. 5.

The binding energy of ethanol is around 45 meV, similar to CH_3Br, but the low-energy peak has a Z_{eff} of ~4400, more than twice that of CH_3Br. Like CH_3Br, all modes are strongly dipole active in this molecule, and so here too the relative peak heights are determined by g_ν alone. Figure 5 shows the model prediction, using frequencies and dipole moments from Ref. [27]. In spite of the size of this molecule, the major features of the Z_{eff} spectrum are reproduced reasonably well. There is a broad feature between 350 and

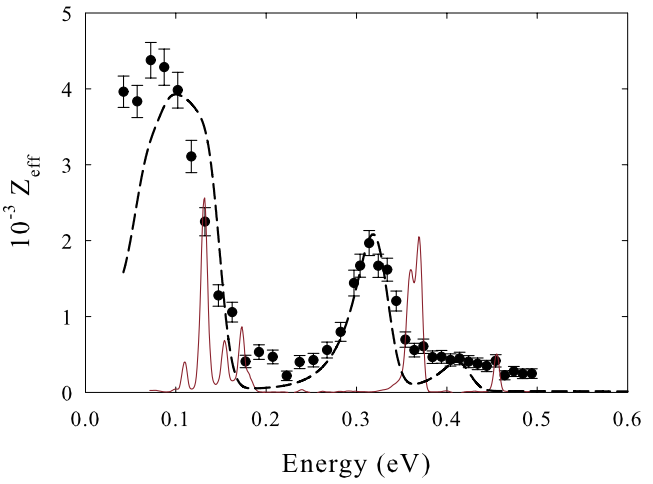

FIG. 5. (Color online) Experimental Z_{eff} for ethanol (●), with the predictions of the Gribakin-Lee model (--) using frequencies and dipole moments from Ref. [27]. Also shown is the normalized infrared absorption (—) from NIST [24].

450 meV in ethanol that may be due to the O-H stretch mode. As discussed in more detail in Sec. VII, a similar feature is observed in methanol and is also attributed to this mode.

V. EVIDENCE OF MULTIMODE EXCITATIONS: THE SPECTRUM OF METHANOL

An example of a molecule where the simple, mode-based VFRs fail to explain the observed Z_{eff} spectrum is methanol (CH_3OH), a substituted methane with the same number of electrons as CH_3F but with one more atom. The experimental Z_{eff} and gas-phase ir absorption spectra for this molecule are shown in Fig. 6. Additional measurements were made in the region from 350 to 450 meV to clarify a new feature.

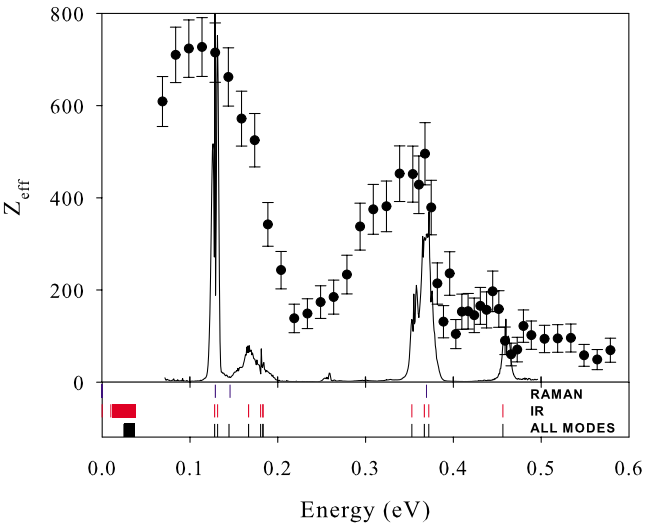

FIG. 6. (Color online) Z_{eff} spectrum of methanol. Also shown is the normalized ir absorption spectrum (—) and the vibrational mode data (vertical bars) from Ref. [24].

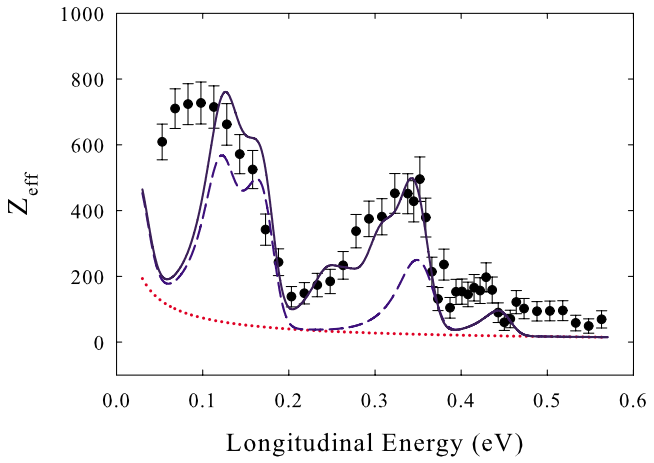

FIG. 7. (Color online) Z_{eff} for methanol, with the predictions of the Gribakin-Lee model adapted to include combination and overtone vibrations. A positron binding energy of 2 meV is assumed for best fit. Reprinted from Ref. [17]. The dotted curve represents the nonresonant (direct) contribution; the dashed line represents the total contribution including only fundamental-mode VFRs; and the solid curve represents the total contribution including both fundamental and multimode VFRs. See text for details.

These data may be slightly mismatched with the rest of the data.

The Z_{eff} spectrum is similar to that of the halomethanes except that the C-H stretch peak is a bit broader, and there is a peak at 430 meV which appears to be due to the O-H stretch vibrational mode. This is the first time that a Z_{eff} feature due to a non-carbon-based vibrational mode has been so clearly observed. According to the NIST webbook [24], the theoretical energy of the O-H stretch mode is 456 meV in gas phase. However, comparisons between liquid and gas-phase ir absorption data indicate that the energy of this vibrational mode may be sensitive to the molecular environment. In particular, it is possible that the presence of a positron causes a reduction in the O-H stretch mode energy, but we do not have an estimate of the size of this effect [17].

While the infrared absorption spectrum is expected to be only weakly correlated with the Z_{eff} peak heights, each infrared peak in Fig. 6 corresponds to a VFR peak. As we now discuss, the enhanced Z_{eff} around 250 meV appears to correspond to the overtone or combination vibrations that can be seen as very small features in the infrared spectrum.

The Gribakin-Lee model was used to calculate the theoretical curves for methanol that are shown in Fig. 7 [17]. The capture widths were calculated using a combination of experimental and theoretical values for the frequencies and dipole moments shown in Table II. When only VFRs from the fundamental modes are included, the result is a narrow C-H stretch peak half the size of the experimental peak. Adjusting the binding energy, which was assumed to be 2 meV for best fit, does not help in resolving this problem; namely, quadrupling this quantity produces the correct C-H stretch-peak height, but makes the low-energy peak too large.

To reconcile this discrepancy between theory and experiment, the coupling to combination and overtone vibrations was included using the dipole strengths from the experimental ir absorption spectra in Ref. [28]. This adjustment results in an enhanced height and width around the C-H stretch peak with little change in the low energy peaks, thus providing much better agreement with the data.

TABLE II. Data for methanol, including the mode energies ω_ν in meV; mode degeneracy factors b_ν, dipole moments d_ν in atomic units; normalization factor $h(\xi)$ (assuming ϵ_b=2 meV), and normalized capture rates $\Gamma^e_\nu/h(\xi)$ in μeV for the vibrational modes. The mode energies ω_ν are from Ref. [24] and dipoles d_ν from Ref. [28], except mode 1 (the CH stretch) and mode 10 (the CH_3 asymmetric deformation), for which the theoretical values of Ref. [29] were used. Mode numbers greater than 12 refer to combination and overtone excitations. A plausible identification for these mode combinations is also indicated, where possible.

Mode	ω_ν	b_ν	d_ν	$h(\xi)$	$\Gamma^e_\nu/h(\xi)$
ν_1	456.4	1	0.0265	0.31	190
ν_2	369.5	1	0.025	0.39	137
ν_3	351.3	1	0.026	0.35	141
ν_4	183.1	1	0.016	0.44	27.8
ν_5	179.8	1	0.011	0.45	12.9
ν_6	176.3	1	0.040	0.45	167
ν_7	138.3	1	0.026	0.49	55.4
ν_8	128.3	1	0.074	0.5	416
ν_9	365.2	1	0.029	0.34	182
ν_{10}	183.1	1	0.016	0.44	27.8
ν_{11}	134.9	1	0.0087	0.49	6.05
ν_{12}	36.58	1	0.087	0.70	164
$\nu_{13}=2\nu_5, \nu_4+\nu_6$	359.6	1	0.027	0.34	155
$\nu_{14}=\nu_5+\nu_6$	357.1	1	0.012	0.34	30.5
$\nu_{15}=2\nu_6$	347.8	1	0.024	0.35	123
$\nu_{16}=\nu_7+\nu_{10}$	321.9	1	0.0086	0.36	14.1
$\nu_{17}=\nu_8+\nu_{10}$	312.7	1	0.016	0.36	47.4
$\nu_{18}=2\nu_7$	276.4	1	0.006	0.38	5.89
$\nu_{19}=2\nu_8$	253.6	1	0.008	0.39	9.61
ν_{20}	161.2	1	0.017	0.46	27.6
ν_{21}	148.8	1	0.018	0.48	28.6

One remaining discrepancy between the model and experiment is the relatively small value of Z_{eff} predicted below 100 meV. A torsion mode at ~40 meV has been included, which causes a slight upturn in Z_{eff} near zero energy. However, it does not have sufficient strength and width to bridge the gap to the next peak at higher energy. According to the NIST webbook, this torsional mode is subject to a "large coupling between internal and overall rotations" [24]. While this effect might allow a shift or redistribution of this peak, the overall spectral weight would still be too small. It is believed that the overtones of this mode might contribute to the spectrum; however, there is, at present, no estimation of the size of this effect.

VI. INCREASING COMPLEXITY: TWO-CARBON MOLECULES AND AMMONIA

While the theory can be adapted to describe methanol, it tends to lose predictive capability with further changes in

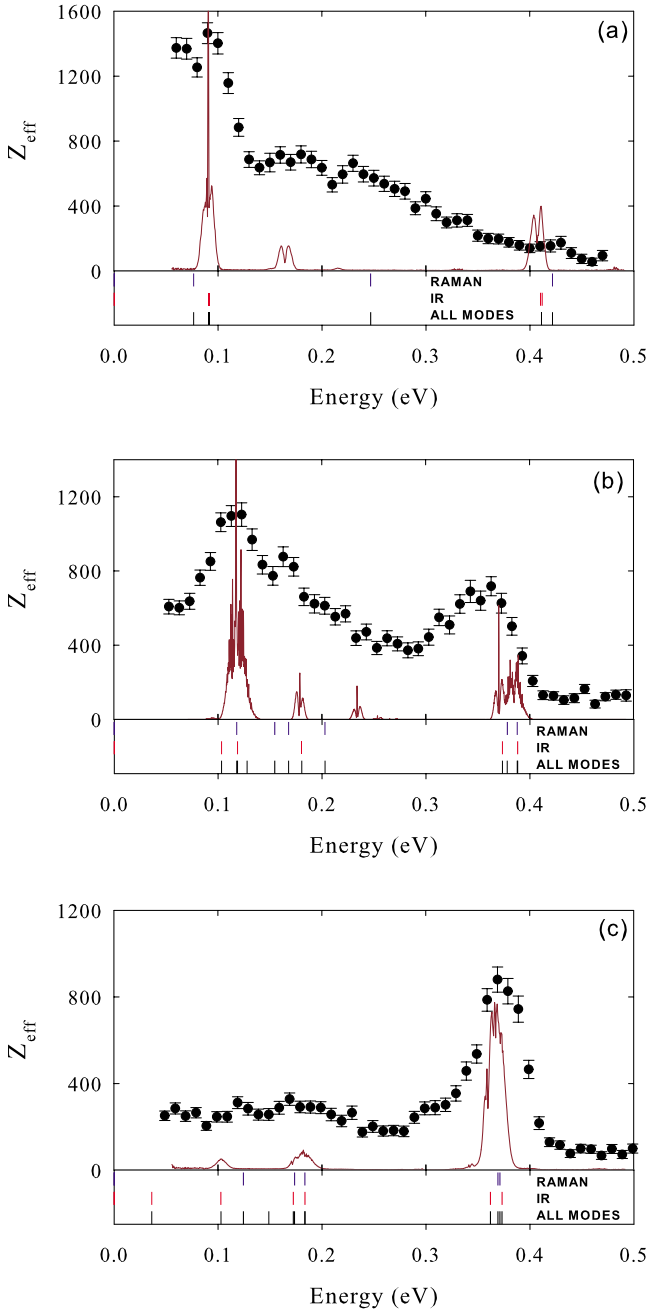

FIG. 8. (Color online) Z_{eff} (●) for (a) acetylene, (b) ethylene, and (c) ethane, reprinted from Ref. [8]. The solid curves (—) show normalized infrared absorption spectra from Ref. [24], and the vertical bars below each plot indicate the fundamental vibrational modes, also from Ref. [24].

molecular size and structure, such as increasing the number of vibrational degrees of freedom. A clear example of this trend is seen in the two-carbon hydrocarbon molecules, acetylene, ethylene, and ethane, for which the Z_{eff} spectra are shown in Fig. 8 [8,9,25]. Acetylene (C_2H_2) has a triple bond, ethylene (C_2H_4) has a double bond, and ethane (C_2H_6) has a single bond.

The shapes of the Z_{eff} spectra in these molecules change with increasing hydrogen saturation. Acetylene is dominated by a low-energy peak with no sign of a C-H stretch peak; ethylene has both peaks; and ethane is dominated by a large C-H stretch peak, with a weaker low-energy plateau. The Z_{eff} spectrum of ethane is closer to that observed in propane and other large alkanes [8,9].

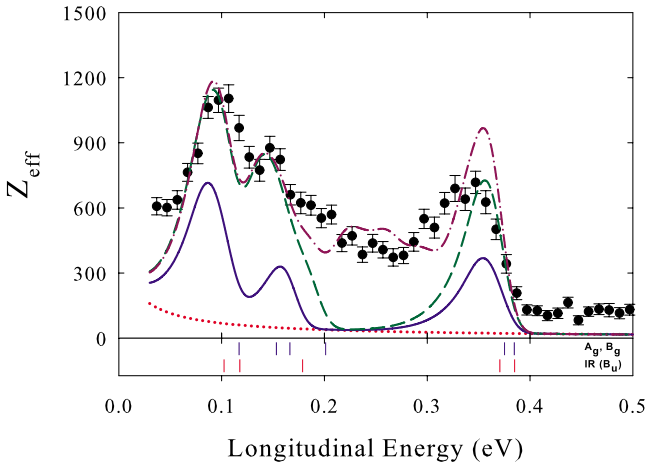

FIG. 9. (Color online) Comparison of Z_{eff} measured for ethylene (●) with Z_{eff} calculated for ϵ_b=10 meV using ir (B_u) modes only (solid); A_g, B_u, and B_g modes (dashed); and these plus ir-active combinations (dot-dashed), in addition to direct annihilation (dots). Vertical bars show the mode energies. Reprinted from Ref. [17].

Of the three two-carbon molecules discussed in this section, ethylene is most easily related to the predictions of the Gribakin-Lee model. The results for this molecule are shown in Fig. 9 [17]. A binding energy of 10 meV has been assumed, based on the position of the experimental C-H stretch peak. Apart from the five ir-active modes (i.e., those with B_u symmetry), there are six other modes (A_g and B_g) that can be populated by s, p, and d wave positrons, as well as 14 ir-active combination vibrations identified from Ref. [30]. For the fundamental vibrations, we set $\Gamma_\nu^e=\Gamma_\nu$, while for the combination VFRs, we set $\Gamma_\nu^e/\Gamma_\nu=1/n$ empirically, where n is the number of single vibrational quanta in the combination, to best match the observed Z_{eff} spectrum [31]. Figure 9 shows that Z_{eff} due to the B_u (ir-active) modes alone considerably underestimates the experimental results. Adding the VFRs of A_g and B_g modes improves the agreement near the peaks, but the annihilation signal in the 0.2–0.3 eV range is still poorly described. As shown in Fig. 9, the theory can match the experiment only by allowing for combination VFRs, which contribute most of the spectral weight above 0.2 eV.

The main difficulty in applying the theory to ethylene is determining the strengths of the many multimode and infrared-forbidden VFRs that are necessary to explain the observed spectrum. However, as shown in Fig. 9, reasonable values of the coupling parameters do produce good agreement between the predictions of the model and experiment.

Similar results are obtained using this procedure for acetylene [32], which has even fewer atoms than methane and its derivatives. The closest molecule to acetylene for which we also have Z_{eff} spectral data is ammonia (NH_3), which also has four atoms. The Z_{eff} spectrum of ammonia is shown in Fig. 10. The spectra for C_2H_2 and NH_3 are, in fact, remarkably similar. In both, there is a low-energy feature, a

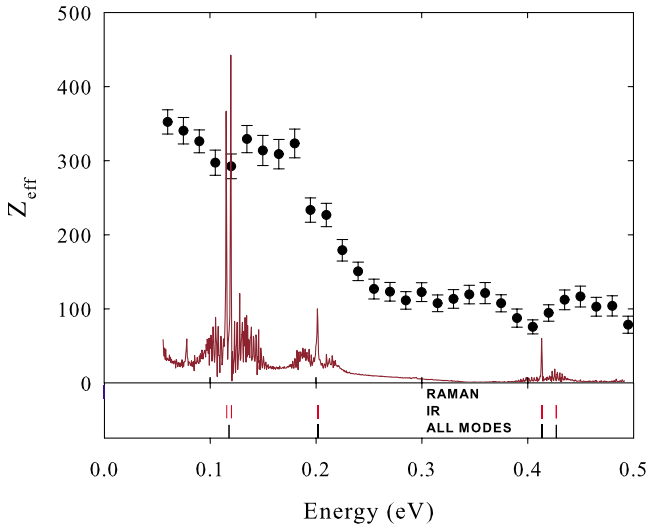

FIG. 10. (Color online) Energy-resolved Z_{eff} and infrared absorption spectra for ammonia reproduced from Ref. [25]. The bars below indicate the positions of vibrational modes (from Ref. [24]).

significant "background" Z_{eff}, and little or no high-energy peak. Acetylene has a thermal Z_{eff} of 3160 [20], which is large enough to suspect the existence of a VFR [14,33]. While the thermal- and energy-resolved Z_{eff} for acetylene are larger than those for ammonia by about a factor of 2, this might be explained by a difference in the modes and the g_ν factors. For instance, assuming low-lying VFRs, the relative magnitudes could be explained if acetylene had a binding of 5 meV and NH_3 had a binding of 1 meV.

While neither acetylene nor ammonia has peaks in Z_{eff} at higher energies, they both appear to have peaks at lower energies, implying that they bind positrons. Both seem to have a strong "background" Z_{eff} which is likely due to overtone or combination vibrational resonances. In fact, the infrared spectrum of acetylene, shown in Fig. 8(a), has weak resonances around 160, 170, and 215 meV, all due to overtones. There is also an infrared-inactive mode around 245 meV. As discussed earlier, accurate calculation of positron coupling to such modes is difficult.

The largest molecule in this series is the alkane, ethane. Like the other two-carbon molecules shown in Fig. 8, ethane has a significant "background" Z_{eff}, especially around 250 meV, where there are no fundamental modes. This is likely due to multimode VFRs. However, ethane also has an unusually large C-H stretch peak and a weak low-energy plateau similar to that of the larger alkanes, such as propane or pentane. This Z_{eff} spectrum is very different than that predicted by the small molecule theory, for which one would expect a C-H stretch peak which is *smaller* than the lower-energy peaks. The binding energy of ethane is close to zero, significantly reducing the predicted magnitudes of all VFRs. In fact, its low-energy Z_{eff} is as weak as that of CH_3F, which has a model-fitted binding energy of 0.3 meV.

The C-H stretch peak in ethane is enhanced by roughly a factor of 5 above the mode-based Gribakin-Lee prediction. In other words, there are effectively 30 modes or mode-combinations contributing to the C-H stretch peak in ethane, even though this molecule only has six C-H stretch modes

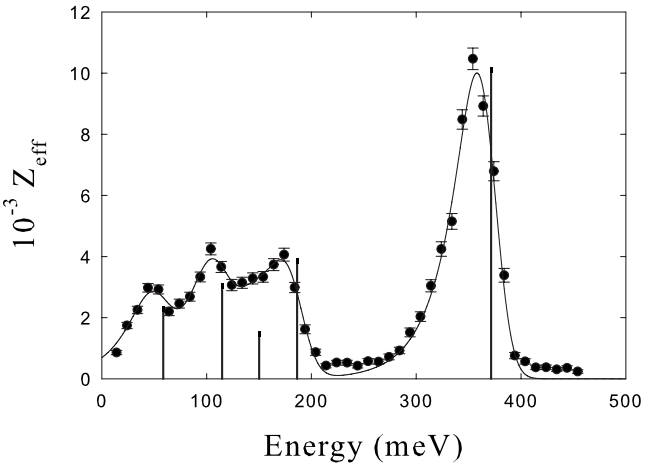

FIG. 11. Energy-resolved Z_{eff} for propane (●) from Ref. [10] with a fit (—) produced by convolving five δ functions with arbitrary amplitudes and positions (vertical lines), with the incident positron energy distribution function. Note that, while the magnitudes of these delta functions exceed greatly the predictions of the Gribakin-Lee theory, they still occur close to fundamental vibrations, after correcting for the ~10 meV binding energy.

and a total of 18 modes. This is probably the same VFR enhancement operative in larger alkanes such as propane (discussed in the next section), in which additional "dark-state" resonances are populated by intramolecular vibrational relaxation [11–13]. Presumably, some critical density of vibrational "dark" states or critical coupling to these states is required to activate this process. In this sense, the number of vibrational degrees of freedom may define a rough boundary between small and large molecule dynamics.

VII. INTRAMOLECULAR VIBRATIONAL ENERGY REDISTRIBUTION AND OTHER EFFECTS

As seen for ethane, while the small-molecule theory works well for molecules with a few atoms, it breaks down quickly as the number of atoms increases. As another example of the effects evident in larger molecules, we consider the case of propane (C_3H_8). Propane data from Ref. [10] are plotted in Fig. 11. Propane exhibits fundamental-mode VFR peaks more than an order of magnitude larger than those predicted by the "one mode–one peak" theory. Furthermore, the dominance of the low-energy resonances, as seen in the halomethanes, is replaced by a dominance of the higher-energy C-H stretch resonance. In this case, the relative Z_{eff} peak heights are no longer determined by the g_ν factors alone.

As shown in Fig. 11, the Z_{eff} spectrum can be fit by convolving a few delta functions with the beam energy distribution function. Note that, while the magnitudes of these peaks greatly exceed the predictions of small molecule theory, they occur at energies close to the expected locations of the fundamental vibrations, after correcting for the binding energy. Interestingly, the spectral shape of Z_{eff}/g_ν is nearly identical for larger alkanes, albeit shifted due to increasing binding energy and increased greatly in magnitude [9,13].

Gribakin has suggested that the number of accessible VFR excitations (and hence the enhancement in Z_{eff}) is effectively increased by IVR [11]. In this model, the energy in an initially excited fundamental vibration, called a "doorway" state, relaxes rapidly into a reservoir of near-degenerate multimode vibrations, often referred to as "dark" states. As a result, the resonant Z_{eff} is greatly enhanced by the local density of these dark states and grows rapidly with the number of vibrational degrees of freedom [12,13].

Because of these qualitative differences in annihilation rates and spectra, we refer to propane as a "large" molecule, while we refer to the halomethanes as "small" molecules. More generally, if the magnitude of the Z_{eff} spectrum can be ascribed to a series of distinct vibrational resonances whose magnitudes are determined entirely by g_ν, then the "small" molecule label is used. If, on the other hand, one must invoke IVR or some other enhancement process, then the "large" molecule label is used.

At the edge of "large" molecule behavior are molecules such as cyclopropane. The Z_{eff} spectra of cyclopropane and propane are compared in Fig. 12. These spectra indicate that the binding energy of both of these molecules is small, i.e., $\sim$10–15 meV. While propane displays the typical Z_{eff} shape of the large alkanes, with a dominant C-H stretch peak and a low-energy plateau of C-H bend and C-C peaks, the Z_{eff} spectrum of cyclopropane has a number of distinctly different features [10].

The C-H stretch peak of cyclopropane is half as large as that of propane, even though it has 3/4 as many C-H stretch modes. The maximum value of Z_{eff} at low energies is about the same as that of propane (i.e., $\sim$400) but only in a narrow region. While the uncertainty in binding may result in differing g_ν factors, this alone cannot explain these differences. As mentioned before, the scaling of Z_{eff} with molecular size can be highly nonlinear. Specifically, the magnitude of Z_{eff} at the C-H stretch peak is observed to scale as $N^{4.1}$, where N is the number of atoms in the molecule [12,13]. We interpret this dependence of Z_{eff} on N to be essentially a power-law dependence on the number of molecular vibrational degrees of freedom of the molecule, $3N-6$. This scaling with N is consistent with the difference in the magnitudes of the C-H stretch peaks in propane and cyclopropane.

The broad low-energy plateau in propane appears as a single peak in cyclopropane. This is probably due to a reduction in VFR-active bending and C-C modes in cyclopropane relative to propane. Since these modes are distributed more sparsely than the C-H stretch modes, it is plausible that the magnitudes of the VFR peaks remain the same, but the number of resonances is reduced. The fact that Z_{eff} does not change for these peaks suggests that the Z_{eff} enhancement mechanism is the same in both.

In the Z_{eff} spectrum of cyclopropane, there is a small feature at 250 meV, between the C-H bend and C-H stretch peaks. This feature occurs in the same region as enhancements in the infrared absorption and is likely due to multimode VFRs [34]. It is interesting that these peaks are so weak. A similar feature is seen in propane. Their magnitudes are more like those of VFRs in small molecules. Perhaps these VFRs are not enhanced as much as the mode-based VFRs in larger molecules. This would explain why multimode VFRs are generally not evident in larger molecules [8–10,13].

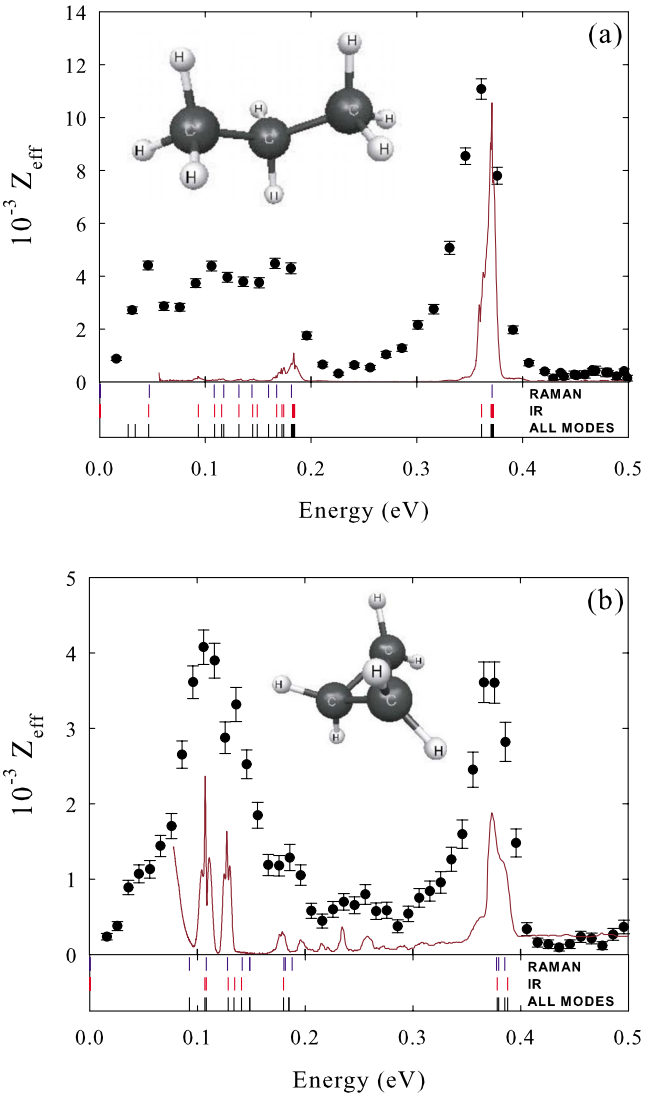

FIG. 12. (Color online) Energy-resolved Z_{eff} (●) for (a) propane and (b) cyclopropane from Ref. [10]. The solid curve (—) represents the normalized ir absorption spectra, and the vertical bars below each plot show the active vibrational mode energies, both from Ref. [24]. Shown as insets are the molecular structures, rendered using data from Ref. [24].

In summary, the predictions of small-molecule theory are in reasonable agreement with the spectra of the substituted methanes, ethanol, acetylene, and ethylene. On the other hand, the magnitudes of Z_{eff} in ethane, cyclopropane, and all of the alkanes with three or more carbons are much larger than can be accounted for by this theory. Presently, the best explanation for this enhancement appears to be some kind of IVR process, as described in Refs. [11–13].

VIII. VFR-WEAK OR INACTIVE MOLECULES

As the binding energy is reduced, the VFR peaks shrink in magnitude proportional to g_ν. According to the small-molecule theory, both the capture rate and the annihilation

rate decrease if the binding energy is very close to zero [16]. Eventually, interference terms (discussed in more detail below) could start to dominate. Finally, the positron bound state disappears and is replaced by a virtual state. In this case, there will be no sharp resonances as VFRs are forbidden. According to Gianturco, a virtual state may lead to long-lived intermediate states during vibrational deexcitation collisions [35], but there is, to date, no clear experimental evidence of such an effect.

One possibility for an unbound positron is a shape resonance. Based upon intuition gained from electron shape resonances, they could manifest themselves as fairly broad peaks in Z_{eff} (e.g., electron shape resonances can be a few eV wide) and could occur in the absence of a positron-molecule bound state or a dipole-allowed vibrational mode. The problem with positron shape resonances (vibrationally enhanced or not) is that it is difficult to produce the required (e.g., centrifugal) barrier in the potential. Low-energy positronic states are thought to have angular momentum $\ell=0$, which tends to preclude such effects. To date, there is a dearth of experimental evidence that such states exist. They have, for example, yet to be observed in any total cross section measurements [36]. We note, however, that there is an interesting prediction of a shape resonance in positron-C_{60} interactions, due to both centrifugal barrier states and cage states [37] that could be tested experimentally with techniques that are presently available. Also, a p-wave shape resonance with $Z_{\mathrm{eff}} \sim 1500$ was predicted in Mg [38].

Below, we discuss a variety of molecules for which the VFRs either do not exist or are too weak to be detected. Many of these molecules exhibit structures in their spectra, but they are unlike those of the VFRs observed to date. Frequently, in fact, only a small change in molecular composition is required to make such a molecule VFR active. For example, as shown in Fig. 13, CH_3F has VFR peaks, while CH_4 (methane) and CF_4 (carbon tetrafluoride) do not [9].

Data for CO_2 are shown in Fig. 14, together with infrared absorption and mode data from NIST [24]. These data were taken allowing the positrons to bounce back and forth through the gas cell for 40 μs instead of 15 μs. While the count rate is improved, systematic errors such as spurious scattering could be enhanced; see Ref. [39] for further details. The spectrum of CO_2 is relatively smooth with no VFRs visible except perhaps at low energies (e.g., $\leqslant$0.1 eV). The spectrum has a baseline value of $\sim$35. Since $Z=22$, this is not too far from that of the uncorrelated electron gas prediction. The contribution of $Z_{\mathrm{eff}}^{(\mathrm{dir})}$ [cf., Eq. (11)] could possibly explain the rise at low energies. The thermal value of Z_{eff} for CO_2 is 54.7 [40]. A vibrational close-coupling calculation by Gianturco and Mukherjee predicts a relatively flat spectrum with no resonances and $Z_{\mathrm{eff}} \sim 50$ [41]. This is in relatively good agreement with the measurements with few assumptions in the model.

As shown in Fig. 14, there is a relatively small but distinct feature (resembling a sawtooth-like oscillation) around 450 meV. The infrared absorption spectra of CO_2 from Ref. [24] indicates a peak at this energy, which seems to be a combination of the symmetric and asymmetric stretch modes. The shape of this feature is unlike a VFR, and it occurs where one might expect a multimode excitation. One possible explanation of this feature arises from the fact that annihilation can have features which parallel those in elastic scattering, namely a resonance that enhances the scattering wave function will also enhance the pick-off annihilation due to positron-electron overlap (even in the absence of positron binding).

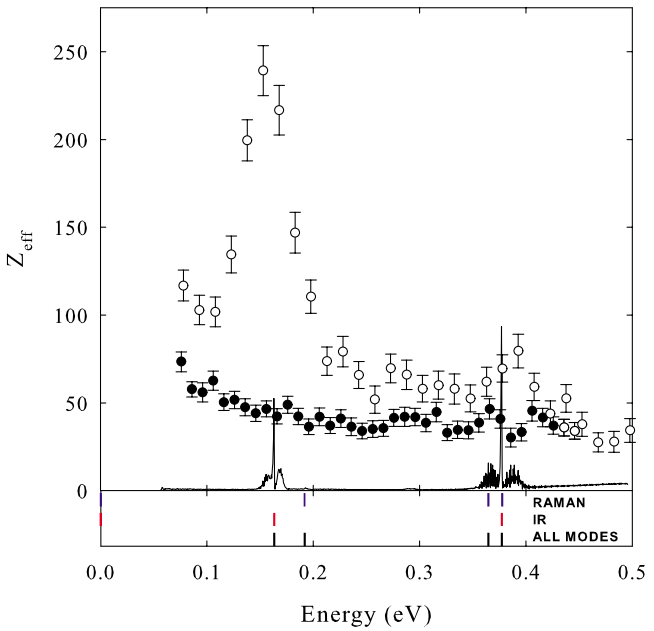

FIG. 13. (Color online) Energy-resolved Z_{eff} for (●) CH_4 and (○) CH_3F from Ref. [9]. The solid curve (—) represents normalized ir absorption spectra for CH_4, and the vertical bars below show the active vibrational mode energies for CH_4, both from Ref. [24]. Note the lack of VFRs in CH_4 as compared to CH_3F.

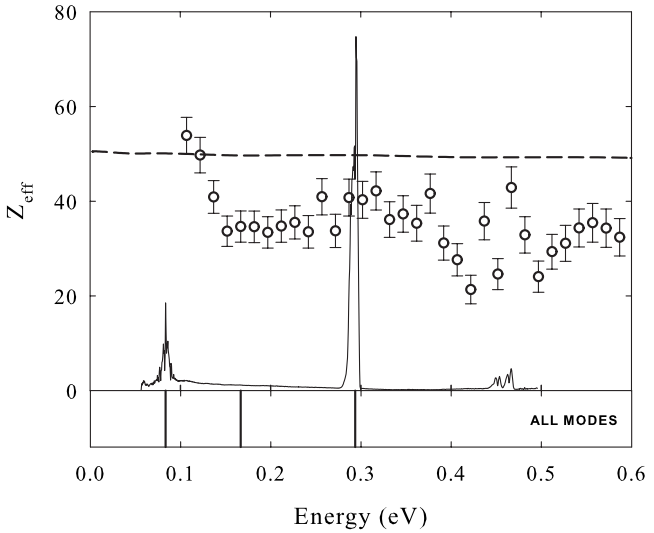

FIG. 14. Energy-resolved Z_{eff} (○) for CO_2, using an extended 40 μs bounce window for improved signal to noise ratio. Note the emergence of new features. The solid curve (—) represents the normalized ir absorption, and the vertical bars below each plot show the active vibrational mode energies, both from Ref. [24]. The dashed curve shows a vibrational close coupling calculation from Ref. [41].

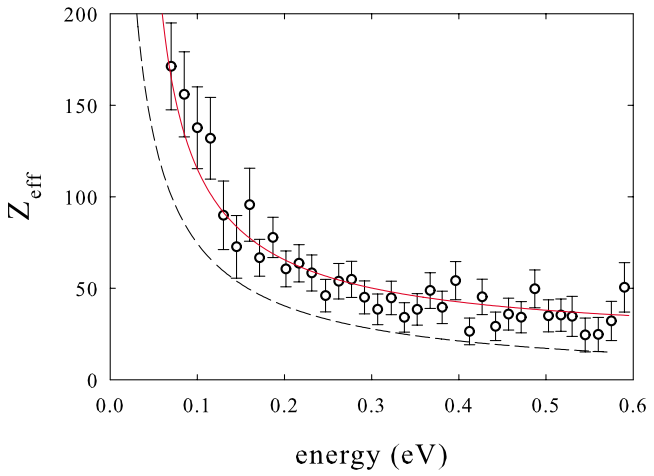

FIG. 15. (Color online) Energy-resolved Z_{eff} (○) for H_2O. The solid curve (—) is a model fit from Eq. (11) for direct Z_{eff}, assuming binding and virtual state energy of 0.3 meV and a constant offset of 20. For comparison, the dashed curve (--) omits this constant offset. See text for details.

Figure 15 shows the Z_{eff} spectrum of water. It decreases monotonically as a function of increasing positron energy with no clear signs of VFRs. Also shown is the predicted contribution of direct annihilation for a low-lying bound state or virtual state from Eq. (11) [32]. While the positron energy resolution is too broad to make a precise determination of the energy of this state, it is on the order of 1 meV or less [42]. A constant offset of 20 was also included in the fit. This corresponds to pick-off annihilation due to the incident (rather than the scattered) positron wave and is referred to as Z_{eff}^0 in Eq. (11) [10,14,15]. Note that water is a polar molecule, so that strictly speaking, Eq. (11) is not applicable. Hence one might view this fit as an empirical parametrization of the energy dependence of Z_{eff}.

Shown in Fig. 16 is a high-resolution spectrum of water taken with a 40 μs bounce window. It exhibits a similar effect to that observed in CO_2, namely, an oscillation in Z_{eff} between 300 and 500 meV. The center of this feature is below the OH stretch mode by nearly 80 meV. It is closer to C-H stretch mode energy in alkanes, although no alkane VFR has that kind of structure. A similar feature occurs in the Z_{eff} spectrum of methane (CH_4) at a lower energy. To amplify this point, in Fig. 16, the feature in methane has been arbitrarily shifted and rescaled in energy to align with the feature in water. The fact that these two Z_{eff} features have such similar shapes seems to indicate a common origin. Calculations by Gianturco indicate that water has a relatively large vibrational excitation cross section with sharp onsets [43]. These channels may be related, either directly or indirectly, to the observed features.

Assuming there is a weakly bound state, there can, in principle, be interference terms between direct and resonant annihilation which are usually omitted [14]. They have the form

$$Z_{\text{eff}}^{(\text{int})} = 2\sqrt{\frac{\pi}{k}}\,\text{Re}\left(\sum_{\nu}\frac{\sqrt{\Gamma_\nu^e}\rho_{ep}^{\nu(\text{int})}}{\epsilon-\omega_\nu+\epsilon_b+i\Gamma_\nu/2}\right), \qquad (12)$$

where

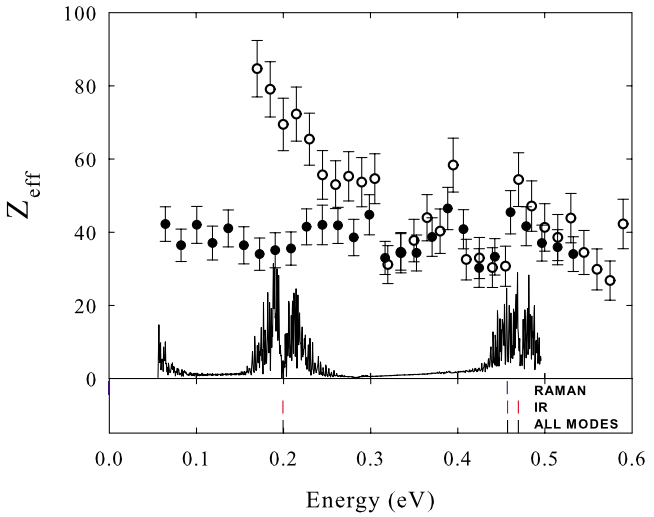

FIG. 16. (Color online) Energy-resolved Z_{eff} (○) for H_2O, using an extended 40 μs bounce window. Note the emergence of new features. The solid curve (—) represents the normalized ir absorption, and the vertical bars below each plot show the active vibrational mode energies, both from Ref. [24]. Also shown is the Z_{eff} spectrum for CH_4 (●) with the energy rescaled as $\epsilon' = 1.8\epsilon - 0.27$ eV (see text for details).

$$\rho_{ep}^{\nu(\text{int})} = \langle\varphi_0(r)\Phi_\nu|\sum_{i=1}^{Z}\delta(\mathbf{r}-\mathbf{r}_i)|e^{i\mathbf{k}\cdot\mathbf{r}}\Phi_0\rangle. \qquad (13)$$

Including these terms can result in features called Fano resonances [44]. These features are interference terms that usually cancel with neighboring features and can be washed out after averaging over the beam energy distribution. However, in the situation described here, there are only one or two modes within the experimental line width. If the VFR magnitude is finite but smaller than, or comparable to the direct annihilation, the interference could be comparable to that of a VFR. At present, it is not possible to say with certainty if the features in either H_2O or CO_2 are due to these effects.

IX. TRENDS IN POSITRON-MOLECULE BINDING ENERGIES

Binding energies derived from VFR positions and other data for a variety of small and medium-sized molecules are summarized in Table III. In the cases where there are VFR peaks but the binding energy is too small to measure, the binding energy is assumed to be nonzero and indicated by "$\gtrsim$0." Where there is no evidence of VFRs, no assignment is made. In this case, positrons may either form barely bound or virtual states. From Table III, one can discern some rough trends when comparing the binding energy to other physical parameters. To lowest order, binding energies tend to increase with molecular size. Larger molecules such as propane (C_3H_8) are more likely to be bound than smaller molecules such as N_2.

For weak binding, the binding energy is related to the positron scattering length $1/\kappa$. If $1/\kappa$ is positive, there is a

TABLE III. Positron binding energy ϵ_b; polarizability α; ionization energy E_i; and permanent dipole μ; for selected small and medium-sized molecules [40,48]. Molecules with no clear VFRs have been assigned a null (—) binding energy. "Threshold" indicates the minimum α and maximum E_i needed for binding in alkali-metal atoms, according to Ref. [21]. Also indicated is the theoretical minimum value of μ needed to ensure a bound state assuming a static dipole [46]. A recent and complementary tabulation of binding energies for 27 larger molecules can be found in Table I of Ref. [13].

Species	ϵ_b (meV)	α (Å^3)	E_i (eV)	μ (D)
		Threshold		
	>0	>2.9	<13.5	>1.625
H_2O	—	1.47	12.61	1.85
N_2	—	1.94	15.98	0
CH_4	—	2.6	12.7	0
CO_2	—	2.66	13.77	0
CF_4	—	2.86	16.25	0
NH_3	$\gtrsim 0$	2.26	10.19	1.47
C_2H_2	$\gtrsim 0$	3.33	11.41	0
CH_3F	$\gtrsim 0$	2.39	12.89	1.86
CH_3OH	$\gtrsim 0$	3.28	10.85	1.70
CH_3Cl	25	4.43	11.22	1.89
CH_3Br	40	5.55	10.54	1.82
C_2H_4	20	4.23	10.51	0
C_2H_6	$\gtrsim 0$	4.44	11.52	0
C_2H_5OH	45	5.11	10.1	1.69
C_3H_8	10	6.29	11.14	0.08

bound state with binding energy $\epsilon_b=\kappa^2/2$, and VFRs can exist with magnitudes proportional to $g=\kappa/k$, where k is the positron momentum. If $1/\kappa$ is negative, the bound state is replaced by a virtual state in the continuum. In both cases, there is a contribution to Z_{eff} from direct annihilation proportional to $(\kappa^2+k^2)^{-1}$ [cf., Eq. (11)] [14,15]. On a related note, there have been some attempts to predict binding energies using a zero-range-potential model, in which κ values are used to parameterize positron interactions with individual atoms or monomers in a molecule [45]. This model successfully predicts the existence of a second positron bound state in large alkanes [13,45]. However, it tends to provide only qualitative agreement with experiment and relies on preknowledge of the monomer κ values.

Another potentially relevant parameter is the permanent dipole moment of the molecule. It is known that a system with a static dipole moment greater than $D_c=1.625$ D has a bound state with either an electron or a positron [46,47]. Indeed, all of the molecules in Table III that meet this criterion, with the exception of water, do appear to have bound states. However, in the absence of additional short-range attraction, the binding energy can be very small and the bound-state wave function very diffuse. As indicated in Table III, the magnitudes of the dipole moments have little correlation with the magnitudes of the binding energies. An example is the methyl halides, all of which have similar dipole moments but very different binding energies. Furthermore, many molecules with no dipole moment show evidence of positron bound states (i.e., by exhibiting VFR annihilation features).

Some insight can be obtained by comparing these trends with calculations of binding energies for atoms. According to a model calculation by Mitroy *et al.* for atoms with one valance electron (i.e., effectively alkali-metal atoms), the positron dynamics are determined entirely by the polarizability α (or equivalently, the ionization potential E_i) [21]. In this model, the positron interacts only with the valence electron in the potential of the atomic core. Binding increases with increasing polarizability and decreasing ionization potential. Furthermore, the minimum polarizability required to bind a positron is ~ 2.9 Å^3, and the maximum ionization energy is ~ 13.5 eV.

As can be seen in Table III, molecules with no clear VFRs (i.e., those with null binding) tend to fall short of these threshold conditions. Conversely, molecules with measurable binding energy or large resonant Z_{eff} (e.g., ethane) more than meet these conditions. The trend of increased binding with increasing halogen size in the halomethanes might also be attributed to increasing polarizability. For either parameter, the dividing line between VFR-active and VFR-inactive molecules is not strict. For instance, the VFR-active molecule CH_3F has a polarizability below this threshold and also lower than that of CF_4. At the same time, CH_3F has a smaller ionization potential than both the threshold value and that of CF_4. Finally, methane meets both threshold conditions but has no apparent VFR.

X. CONCLUDING REMARKS

While there is considerable variation in the features due to positron annihilation in small molecules, there are now important cases where theory and experiment have converged. Namely, Gribakin and Lee have developed an excellent, quantitative theory for VFR-mediated annihilation in small molecules for situations in which all vibrational modes are infrared active. The only remaining free parameter is the positron-molecule binding energy that, at present, must be taken from experimental measurements. Prototypical examples described here are the halomethanes and the deuterated halomethanes.

This model has also been extended to include infrared-active overtones and combination vibrations as well as modes with different symmetries. The model works well for methanol, where the multimode coupling strengths can either be calculated or taken from ir measurements. However, it is difficult to calculate the coupling for weak multimode excitations, and so the predictions for molecules such as acetylene and ethylene are only in qualitative agreement with the measurements. In these cases, one is forced to make ad hoc decisions as to which additional resonances should be counted and the weights ascribed to each. When the size of the molecule increases further, the Z_{eff} values increase rapidly, and the Z_{eff} spectra become even more difficult to predict, presumably due to effects such as IVR.

An important open question is why these multimode and infrared-inactive VFRs are present in some small molecules

such as methanol, ethylene, and acetylene, but absent from others, such as the halomethanes and ethanol. According to the Gribakin-Lee theory, any excitation with a capture rate greater than the very small annihilation rate can be expected to produce a measurable VFR. Table II shows that the capture rates of some combinations and overtones can be reasonably large—within an order of magnitude of the rates for the fundamental vibrations. For reference, the average ratio Γ_ν^e/Γ^a for fundamental vibrations in methanol is only five times larger than it is in CH_3Cl. Therefore, without an additional suppression mechanism, multimode VFRs might be expected to be both more prevalent and more prominent.

To suppress a VFR in the present framework, the capture rate must be lowered to or below Γ^a, or an additional escape channel must be introduced. At present, it is unclear how either of these conditions can be met for multimode VFRs alone. Based upon observations in larger molecules, inelastic escape channels appear to be inoperative [12,13]. The internal annihilation rate cannot be changed as this would result in a change in F, which determines the overall magnitude of all of the resonances. This leaves Γ_ν^e, which cannot be reduced without significantly altering the present theory.

An important transition in behavior occurs in ethane. This molecule has a large C-H stretch resonance whose magnitude exceeds greatly predictions within the framework of the theory. For this reason, we classify ethane as a "large" molecule, apparently governed by additional (i.e., IVR) dynamics that result in further enhancements in Z_{eff}. Propane and cyclopropane are also in this class, as are larger hydrocarbon molecules [12,13]. Interestingly, this strong enhancement is not observed for the multimode VFRs, which are either absent or very weak in most larger molecules.

Data were presented for molecules with no identifiable VFR features, such as water and CO_2, suggesting that positrons may not bind to these molecules. However, some of these molecules also exhibit tantalizing structures in their annihilation spectra. Possible explanations for these features include resonances in the pick-off annihilation, VFR-direct interference terms, and vibrationally enhanced shape resonances.

A continuing challenge is the development of a quantitative understanding of positron-molecule binding energies, which so far have only been calculated for molecules with permanent dipole moments greater than the critical value [49–55]. A model calculation for positron binding to alkali-metal atoms [21] potentially provides some insight in this regard; namely, it supplies the approximate conditions for positron binding, at least in atoms, in terms of the polarizability and ionization energy. Beyond these empirical insights, there are no rigorous calculations of positron binding that can be compared with the available experimental data. Thus, a predictive understanding of which molecules bind positrons and the magnitudes of positron-molecule binding energies remains as a continuing challenge for both theorists and experimentalists.

ACKNOWLEDGMENTS

We wish to acknowledge extensive discussions with G. F. Gribakin on many aspects of this work, helpful conversations with C. M. R. Lee, J. P. Marler, and J. R. Danielson, and the expert assistance of E. A. Jerzewski. This work is supported by the National Science Foundation Grant No. 02-44653.

[1] P. J. Schultz and K. G. Lynn, Rev. Mod. Phys. **60**, 701 (1988).
[2] M. Charlton and J. Humberston, *Positron Physics* (Cambridge University Press, New York, 2001).
[3] C. M. Surko, G. F. Gribakin, and S. J. Buckman, J. Phys. B **38**, R57 (2005).
[4] D. A. L. Paul and L. Saint-Pierre, Phys. Rev. Lett. **11**, 493 (1963).
[5] G. R. Heyland, M. Charlton, T. C. Griffith, and G. L. Wright, Can. J. Phys. **60**, 503 (1982).
[6] C. M. Surko, A. Passner, M. Leventhal, and F. J. Wysocki, Phys. Rev. Lett. **61**, 1831 (1988).
[7] K. Iwata, R. G. Greaves, T. J. Murphy, M. D. Tinkle, and C. M. Surko, Phys. Rev. A **51**, 473 (1995).
[8] S. J. Gilbert, L. D. Barnes, J. P. Sullivan, and C. M. Surko, Phys. Rev. Lett. **88**, 043201 (2002).
[9] L. D. Barnes, S. J. Gilbert, and C. M. Surko, Phys. Rev. A **67**, 032706 (2003).
[10] L. D. Barnes, J. A. Young, and C. M. Surko, Phys. Rev. A **74**, 012706 (2006).
[11] G. F. Gribakin and P. M. W. Gill, Nucl. Instrum. Methods Phys. Res. B **221**, 30 (2004).
[12] J. A. Young and C. M. Surko, Phys. Rev. Lett. **99**, 133201 (2007).
[13] J. A. Young and C. M. Surko, Phys. Rev. A **77**, 052704 (2008).
[14] G. F. Gribakin, Phys. Rev. A **61**, 022720 (2000).
[15] G. Gribakin, in *New Directions in Antimatter Physics and Chemistry*, edited by C. M. Surko and F. A. Gianturco (Kluwer Academic Publishers, Dordrecht, 2001), pp. 413–435.
[16] G. F. Gribakin and C. M. R. Lee, Phys. Rev. Lett. **97**, 193201 (2006).
[17] J. A. Young, G. F. Gribakin, C. M. R. Lee, and C. M. Surko, Phys. Rev. A **77**, 060702(R) (2008).
[18] Y. N. Demkov and V. N. Ostrovskii, *Zero-Range Potentials and Their Applications in Atomic Physics* (Plenum Press, New York, 1988).
[19] M. W. Schmidt *et al.*, J. Comput. Chem. **14**, 1347 (1993).
[20] K. Iwata, R. G. Greaves, and C. M. Surko, Phys. Rev. A **55**, 3586 (1997).
[21] J. Mitroy, M. W. J. Bromley, and G. Ryzhikh, J. Phys. B **32**, 2203 (1999).
[22] J. Mitroy and I. A. Ivanov, Phys. Rev. A **65**, 042705 (2002).
[23] L. D. Barnes, J. P. Marler, J. P. Sullivan, and C. M. Surko, Phys. Scr., T **110**, 280 (2004).
[24] NIST Chemistry WebBook, http://webbook.nist.gov/chemistry/
[25] L. D. Barnes, Ph.D. thesis, University of California, San Diego, 2005.

[26] G. F. Gribakin and C. M. R. Lee (private communication).
[27] R. A. Shaw, H. Wieser, R. Dutler, and A. Rauk, J. Am. Chem. Soc. **112**, 5401 (1990).
[28] J. E. Bertie and S. L. Zhang, J. Mol. Struct. **333**, 413 (1997).
[29] J. Florian, J. Leszczynski, B. G. Johnson, and L. Goodman, Mol. Phys. **91**, 439 (1997).
[30] R. Georges, M. Bach, and M. Herman, Mol. Phys. **97**, 279 (1999).
[31] A possible physical reason for this is that combination vibration VFRs can have more than one positron emission channel, increasing their total widths, so that $\Gamma_\nu^e < \Gamma_\nu$.
[32] G. F. Gribakin (private communication).
[33] C. R. C. de Carvalho, Marcio T. do N. Varella, M. A. P. Lima, and E. P. da Silva, Phys. Rev. A **68**, 062706 (2003).
[34] G. F. Gribakin (private communication).
[35] T. Nishimura and F. A. Gianturco, Phys. Rev. Lett. **90**, 183201 (2003).
[36] J. P. Sullivan, S. J. Gilbert, S. J. Buckman, and C. M. Surko, J. Phys. B **34**, L467 (2001).
[37] F. A. Gianturco and R. R. Lucchese, Phys. Rev. A **60**, 4567 (1999).
[38] J. Mitroy and M. W. J. Bromley, Phys. Rev. Lett. **98**, 173001 (2007).
[39] J. A. Young, Ph.D. thesis, University of California, San Diego, 2007.
[40] K. Iwata, Ph.D. thesis, University of California, San Diego, 1997.
[41] F. A. Gianturco and T. Mukherjee, Europhys. Lett. **48**, 519 (1999).
[42] The fit shown in Fig. 15 assumes a binding or virtual state energy of 0.3 meV.
[43] T. Nishimura and F. A. Gianturco, Eur. Phys. J. D **33**, 221 (2005).
[44] U. Fano, Phys. Rev. **124**, 1866 (1961).
[45] G. F. Gribakin and C. M. R. Lee, Nucl. Instrum. Methods Phys. Res. B **247**, 31 (2006).
[46] O. H. Crawford, Proc. Phys. Soc. London **91**, 279 (1967).
[47] M. Tachikawa, R. J. Buenker, and M. Kimura, J. Chem. Phys. **119**, 5005 (2003).
[48] *CRC Handbook of Chemistry and Physics*, 85th ed. edited by D. R. Linde (CRC Press, Boca Raton, FL, 2004).
[49] K. Strasburger, J. Chem. Phys. **114**, 615 (2001).
[50] J. Mitroy, M. W. J. Bromley, and G. G. Ryzhikh, J. Phys. B **35**, R81 (2002).
[51] J. R. Mohallem, F. Rolim, and C. P. Gonalves, J. Phys. B **37**, 1045 (2004).
[52] M. Tachikawa, R. J. Buenker, and M. Kimura, J. Chem. Phys. **121**, 9191 (2004).
[53] R. J. Buenker, H. P. Liebermann, V. Melnikov, M. Tachikawa, L. Pichland, and M. Kimura, J. Phys. Chem. A **109**, 5956 (2005).
[54] F. A. Gianturco, J. Franz, R. J. Buenker, H.-P. Liebermann, L. Pichl, J.-M. Rost, M. Tachikawa, and M. Kimura, Phys. Rev. A **73**, 022705 (2006).
[55] R. J. Buenker, H. P. Liebermann, L. Pichl, M. Tachikawa, and M. Kimura, J. Chem. Phys. **126**, 104305 (2007).